

Fermi-surface topology of the heavy-fermion system Ce_2PtIn_8

J. Klotz,^{1,2,*} K. Götze,^{1,2,†} E. L. Green,¹ A. Demuer,³ H. Shishido,⁴ T. Ishida,⁴ H. Harima,⁵ J. Wosnitzer,^{1,2} and I. Sheikin^{3,‡}

¹*Hochfeld-Magnetlabor Dresden (HLD-EMFL), Helmholtz-Zentrum Dresden-Rossendorf, 01328 Dresden, Germany*

²*Institut für Festkörper- und Materialphysik, Technische Universität Dresden, 01069 Dresden, Germany*

³*Laboratoire National des Champs Magnétiques Intenses (LNCMI-EMFL), CNRS, UGA, 38042 Grenoble, France*

⁴*Osaka Prefecture University, Department of Electronics,*

Mathematics, and Physics, Sakai, Osaka 5998531, Japan

⁵*Graduate School of Science, Kobe University, Kobe 657-8501, Japan*

(Dated: October 21, 2021)

Ce_2PtIn_8 is a recently discovered heavy-fermion system structurally related to the well-studied superconductor CeCoIn_5 . Here, we report on low-temperature de Haas-van Alphen-effect measurements in high magnetic fields in Ce_2PtIn_8 and Pr_2PtIn_8 . In addition, we performed band-structure calculations for localized and itinerant Ce-4f electrons in Ce_2PtIn_8 . Comparison with the experimental data of Ce_2PtIn_8 and of the 4f-localized Pr_2PtIn_8 suggests the itinerant character of the Ce-4f electrons. This conclusion is further supported by the observation of effective masses in Ce_2PtIn_8 , which are strongly enhanced with up to 26 bare electron masses.

I. INTRODUCTION

Unconventional superconductivity in the vicinity of quantum-critical points (QCPs) is an intensely-studied phenomenon in Ce-based heavy-fermion (HF) systems. Among these materials, CeCoIn_5 exhibits the highest known superconducting transition temperature $T_c = 2.3 \text{ K}^{1,2}$. Several theoretical works suggest that the presence of two-dimensional (2D) Fermi surface (FS) sheets enhances antiferromagnetic (AFM) fluctuations which are believed to be responsible for Cooper-pair formation in HF compounds³⁻⁸. Indeed, CeCoIn_5 possesses almost cylindrical FS sheets at low temperatures, where Ce-4f electrons become itinerant⁹⁻¹¹.

Structurally, CeCoIn_5 belongs to the family of $\text{Ce}_n\text{T}_m\text{In}_{3n+2m}$ (T: transition metal, $n = 1, 2, 3$, $m = 0, 1, 2$). Unit cells within this family are composed of n layers of conducting CeIn_3 separated by m layers of insulating TIn_2 , as shown in Fig. 1. By increasing the ratio m/n , the spacing between the CeIn_3 building blocks becomes larger, which is expected to augment 2D behavior. Therefore, controlling the m/n ratio enables a systematic study of the relation between FS dimensionality and superconducting properties.

Here, we focus on the platinum members of the family, i.e., $\text{Ce}_n\text{Pt}_m\text{In}_{3n+2m}$. So far, CeIn_3 , $\text{Ce}_3\text{PtIn}_{11}$, Ce_2PtIn_8 ,¹² and CePt_2In_7 ¹³ have been successfully synthesized. Inside this group, CeIn_3 has the lowest m/n ratio and a cubic crystal structure. Thus, it is expected to host the most three-dimensional (3D) FS sheets, which is supported by both the band-structure calculations¹⁴ and de Haas-van Alphen (dHvA) experiments^{15,16}. CeIn_3 becomes superconducting with $T_c = 0.2 \text{ K}$ at a critical pressure $P_c = 2.5 \text{ GPa}^4$. Increasing the pressure beyond P_c changes the character of the Ce-4f electrons from localized to itinerant¹⁴.

On the other end, CePt_2In_7 has the highest m/n ratio and is, therefore, expected to be the most 2D compound

in the $\text{Ce}_n\text{Pt}_m\text{In}_{3n+2m}$ series. This assumption was ascertained by quantum-oscillation measurements and band-structure calculations¹⁷⁻¹⁹. Measurements employing a tunnel-diode-oscillator technique in pulsed magnetic fields gave evidence for the existence of localized 4f electrons only above an anomaly at $B_m = 45 \text{ T}^{17}$. Subsequent experiments clarified that the localized character also persists at lower fields^{18,19}. Superconductivity in CePt_2In_7 emerges around a pressure-induced suppression of the AFM ground state at $P_c = 3.2\text{-}3.5 \text{ GPa}$ with $T_c = 2.1 \text{ K}^{20-22}$.

Intermediate m/n ratios are realized in $\text{Ce}_3\text{PtIn}_{11}$ and Ce_2PtIn_8 , which have been synthesized for the first time only recently¹². $\text{Ce}_3\text{PtIn}_{11}$ exhibits AFM order below $T_N = 2.2 \text{ K}$ and, unlike CeIn_3 and CePt_2In_7 , becomes superconducting already at ambient pressure with $T_c = 0.32 \text{ K}$, which increases to $T_c = 0.7 \text{ K}$ at $P_c = 1.3 \text{ GPa}^{23}$. In addition, its large Sommerfeld coefficient $\gamma_{el} = 520 \text{ mJ/molK}^2$ indicates the HF nature of this compound²³. Due to the novelty of Ce_2PtIn_8 , there are, to the best of our knowledge, no publications addressing its ground state so far. However, the isostructural non-magnetic compound Ce_2PdIn_8 is known to become superconducting at $T_c = 0.7 \text{ K}^{24-28}$. The same crystal structure is also realized in Ce_2TIn_8 with $T = \text{Co, Rh, Ir}$. Two of these compounds are HF superconductors: Ce_2CoIn_8 ($T_c = 0.4 \text{ K}$, $\gamma_{el} = 1 \text{ J/molK}^2$)²⁹ and Ce_2RhIn_8 ($T_c = 2 \text{ K}$ at $P_c \approx 0.4 \text{ GPa}^{30}$, $\gamma_{el} = 800 \text{ mJ/molK}^{231}$). The third compound, Ce_2IrIn_8 , is also a HF system ($\gamma_{el} = 1.4 \text{ J/molK}^2$). In this material, no superconducting or magnetic order was found down to 50 mK^{32} , but a non-Fermi-liquid behavior was observed in applied magnetic fields³³. For all three compounds, quantum-oscillation measurements and/or angle-resolved photoemission spectroscopy revealed quasi-2D FSs^{31,34-36}.

The most direct way to establish the FS topology are quantum-oscillation measurements. In this paper, we report on high-field dHvA measurements of Ce_2PtIn_8 . Comparing the results to band-structure calculations

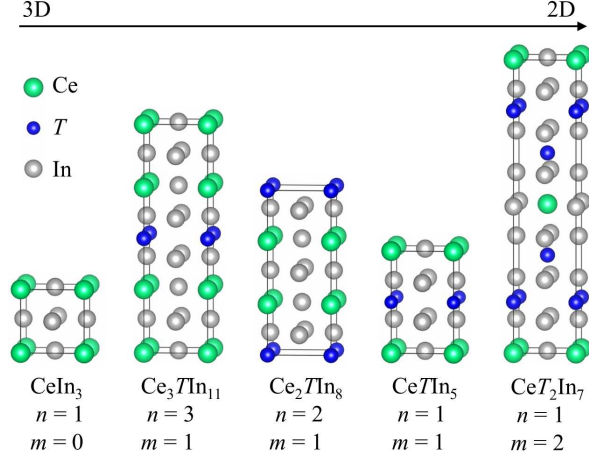


FIG. 1. Crystal structure of the $Ce_n T_m In_{3n+2m}$ family, sorted by increasing m/n ratio.

and to our dHvA data of the $4f$ -localized counterpart Pr_2PtIn_8 evidences itinerant $Ce-4f$ electrons in Ce_2PtIn_8 . Furthermore, our data reveal the existence of a large, 2D FS sheet in this compound. Albeit being less corrugated than its FS counterpart in the isostructural superconductor Ce_2PdIn_8 , there is no signature of superconductivity in the torque data of Ce_2PtIn_8 . We also determined the effective masses of Ce_2PtIn_8 , yielding values between $3.3m_e$ and $25.7m_e$, where m_e is the bare electron mass.

II. EXPERIMENTAL

Single crystals of Ce_2PtIn_8 and Pr_2PtIn_8 were grown using the In self-flux method. A detailed description of the growth conditions can be found in Ref. [37]. Both samples used in our study were investigated by Laue diffraction. All the spots we observed in the diffraction images originate from Ce_2PtIn_8 and Pr_2PtIn_8 , respectively. However, it was previously demonstrated that Ce_2PtIn_8 single crystals grown by In self-flux technique often contain Ce_3PtIn_{11} and $CeIn_3$ impurities, the amount of which depends on the growing conditions¹². We have, therefore, measured the specific heat of our Ce_2PtIn_8 sample by relaxation technique in the temperature range from 1.8 to 30 K. The total heat capacity, C , divided by temperature, T , of the 125 μg sample is shown in Fig. 2. We have indeed observed two anomalies at 2 and 10 K, which coincide with the AFM transitions in Ce_3PtIn_{11} ^{12,23} and $CeIn_3$ ¹⁴, respectively. The size of these anomalies, $\Delta C/T \simeq 1.4 \times 10^{-8} \text{ J/K}^2$, is small compared to the large specific-heat jumps at T_N in pure Ce_3PtIn_{11} ($\Delta C/T = 2.4 \text{ J/mol K}^2$)^{12,23} and $CeIn_3$ ($\Delta C/T = 1.1 \text{ J/mol K}^2$)¹⁴. We, thus, estimate that our Ce_2PtIn_8 sample contains a mass fraction of approximately 8 % Ce_3PtIn_{11} and 5 % $CeIn_3$ impurities. This

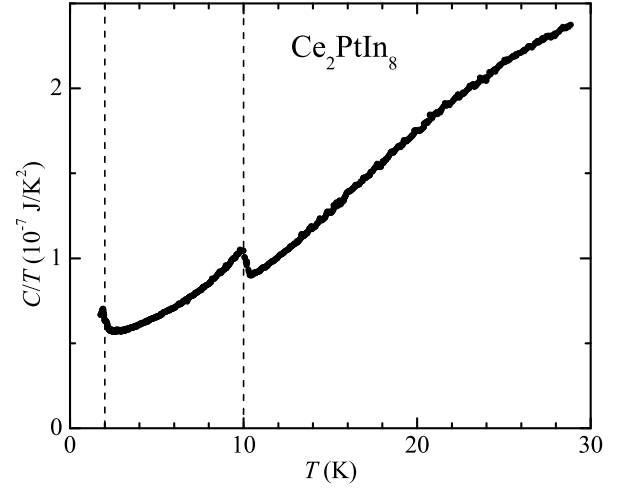


FIG. 2. Total heat capacity divided by temperature of the 125 μg Ce_2PtIn_8 crystal. Dashed lines indicate the known transition temperatures of $CeIn_3$ and Ce_3PtIn_{11} .

is taken into account during the data analysis, and does not affect our main conclusions. After subtracting impurity contributions, we estimated a Sommerfeld coefficient $\gamma = 0.5 \text{ J/mol K}^2$.

Angle-dependent quantum-oscillation measurements were performed on the same sample using capacitive torque magnetometry, employing 25 μm and 50 μm thick CuBe cantilevers. The experiments were conducted in a dilution refrigerator with a base temperature of about 30 mK. High magnetic fields up to 34 T were provided by a resistive magnet in the LNCMI-Grenoble.

III. RESULTS AND DISCUSSION

A. dHvA measurements of Ce_2PtIn_8

Figure 3(a) shows a typical torque signal for Ce_2PtIn_8 taken at an angle $\Theta_{010} = 2^\circ$ after subtracting the non-oscillatory background. Throughout this paper, all angles are measured from the crystallographic c axis. The quantum oscillations are clearly visible. By performing a Fourier transformation, we obtained the corresponding frequency spectrum shown in Fig. 3(b). There are six fundamental frequencies, denoted as α_1 , α_2 , γ , δ , ϵ , and κ . Details of the angular dependence of the dHvA frequencies will be discussed in Sec. III C, together with the results of the band-structure calculations. No signatures of phase transitions were observed in any of the torque signals.

B. Band-structure calculations

In order to determine whether the $4f$ electrons are itinerant or localized, we performed band-structure calcula-

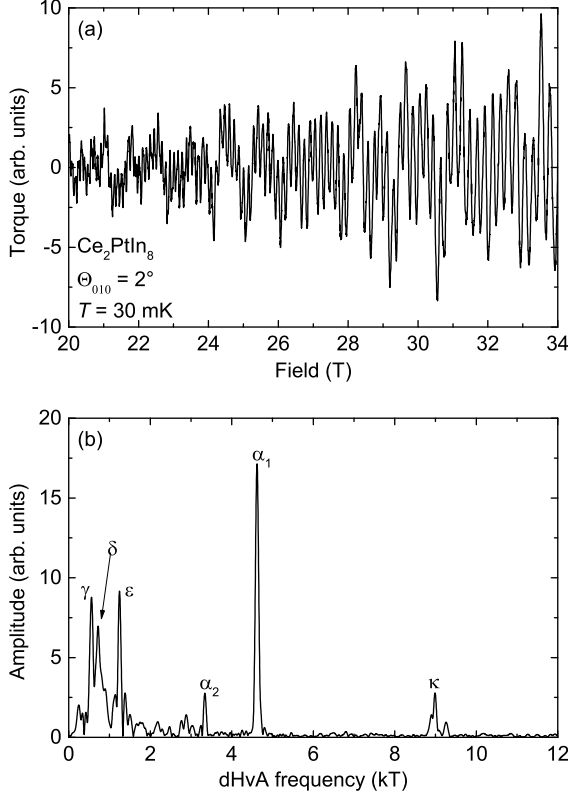


FIG. 3. (a) Torque signal of Ce_2PtIn_8 after subtracting a non-oscillatory background signal. (b) Corresponding frequency spectrum obtained by a Fourier transform of the data shown in (a).

tions using the KANSAI code, based on an FLAPW (full potential linear augmented plane wave) method with a local density approximation (LDA). The relativistic effect is considered by using the technique proposed by Koelling and Harmon³⁸. The spin-orbit coupling is included as the second variational procedure for valence electrons.

In the calculations, we used the lattice parameters of $a = 4.6893 \text{ \AA}$ and $c = 12.1490 \text{ \AA}$, taken from Ref. [12]. Structure parameters are 0.30795 for the $2d$ site of Ce, 0.12241 for the $4i$ site of In, and 0.3072 for the $2h$ site of In. Core electrons (Xe core minus $5s^25p^6$ electrons for Ce/La, Xe core minus $5p^6$ plus $4f^{14}$ for Pt, Kr core for In) are calculated inside the Muffin-Tin spheres in each self-consistent step. $5s^25p^6$ electrons on Ce/La, $5p^6$ electrons on Pt, and $4d^{10}$ electrons on In are calculated as valence electrons by using a second energy window. The LAPW basis functions are truncated at $|k + G_i| \leq 4.20 \times 2\pi/a$, corresponding to 821 LAPW functions. The sampling points are 220 k -points uniformly distributed in the irreducible $1/16$ th of the Brillouin zone, which are divided by (18, 18, 6).

In order to improve the agreement between the calculations and our Ce_2PtIn_8 dHvA data, the Ce- $4f$ states are shifted upward by 0.2 Ry from LDA. To compare

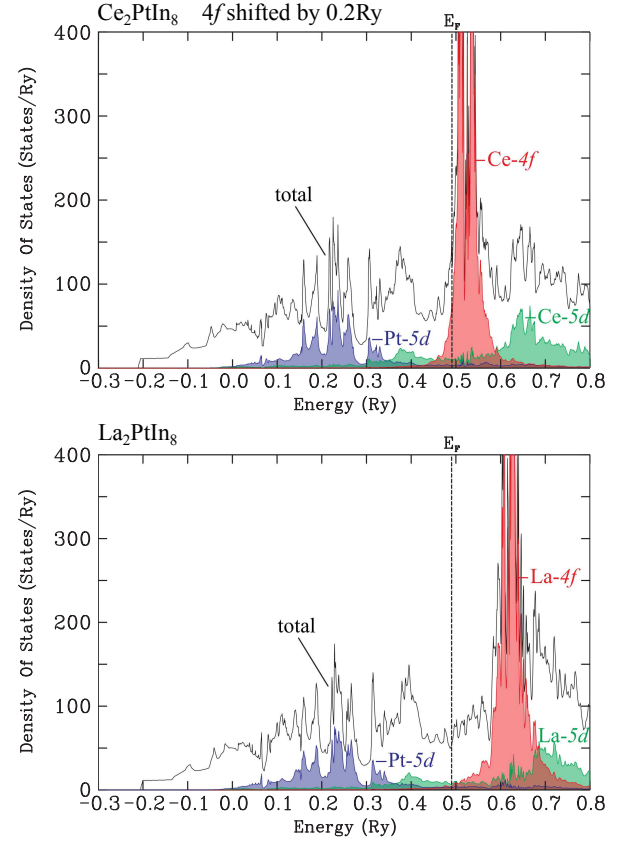


FIG. 4. Calculated densities of states for Ce_2PtIn_8 (top) and La_2PtIn_8 (bottom). Dashed lines indicate the Fermi energy E_F .

the non- f reference or localized $4f$ electrons model, the calculation for La_2PtIn_8 was also performed by using the structural parameters of Ce_2PtIn_8 as crystals of La_2PtIn_8 are currently unavailable. For both itinerant and localized $4f$ electrons, the resulting densities of states and band structures are shown in Figs. 4 and 5, respectively. The corresponding Fermi surfaces are shown in Fig. 6.

C. Experimental data of Ce_2PtIn_8 vs. band-structure calculations

The comparison of the experimentally determined dHvA frequencies in Ce_2PtIn_8 and the calculated frequencies for La_2PtIn_8 and Ce_2PtIn_8 is shown in Fig. 7. Overall, we observed eight dHvA frequency branches, denoted by α , γ , δ , ε , ζ , η , κ , and ω . One of these branches, α , could be traced up to 70° away from the c axis. Roughly following a $1/\cos(\Theta)$ behavior, it indicates the existence of a quasi-2D corrugated cylindrical FS sheet. In addition, a multitude of frequencies lower than 2 kT suggests the existence of several small FS pockets. Two of these frequencies, ε and η , were observed over the entire angular range. Surprisingly, we also observed a fairly large and almost spherical FS sheet, evidenced by

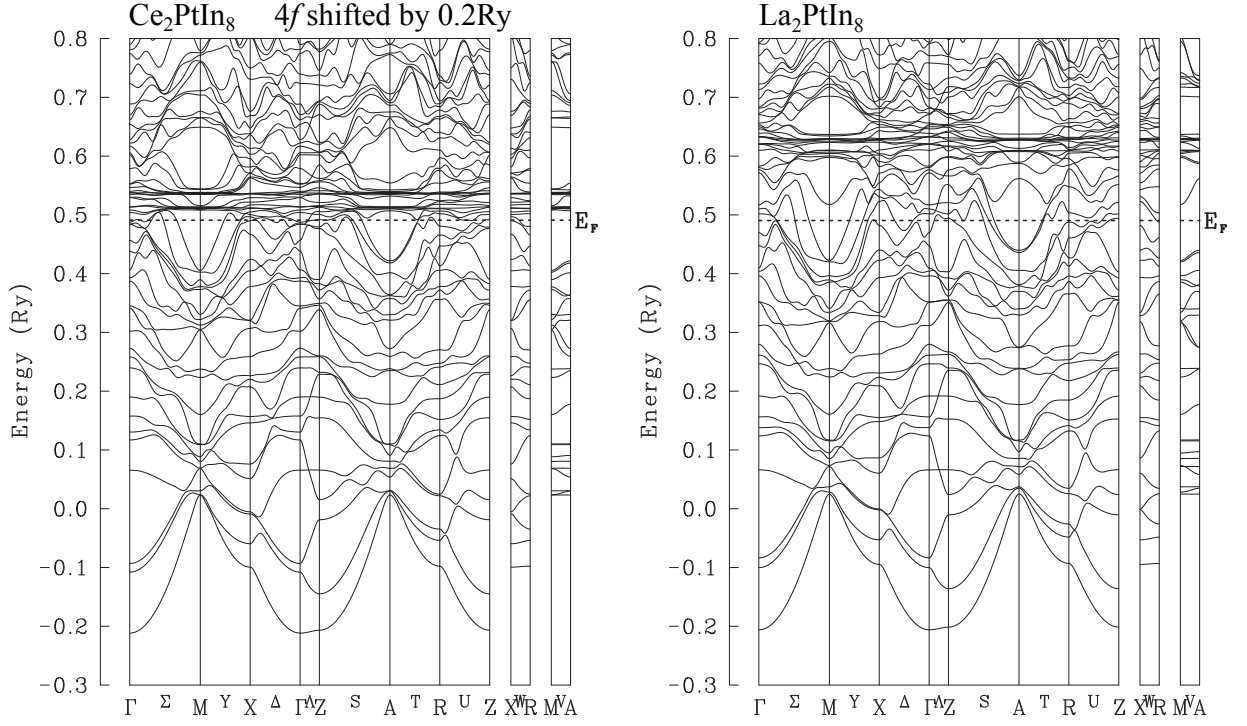


FIG. 5. Calculated band structures along high-symmetry axes for Ce_2PtIn_8 (left) and La_2PtIn_8 (right). Dashed lines indicate the Fermi energy E_F .

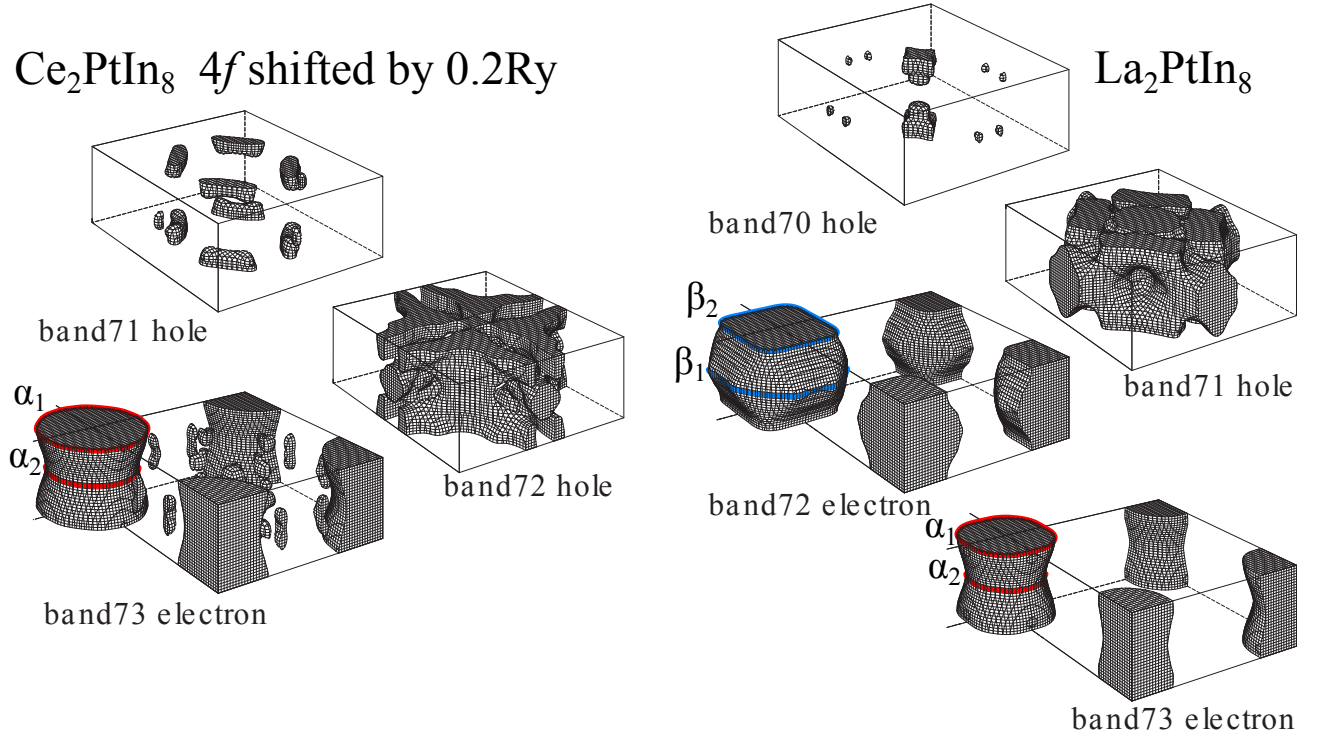


FIG. 6. Calculated FSs for Ce_2PtIn_8 (left) and La_2PtIn_8 (right). Solid lines indicate the extremal cross-sections of quasi-2D FS sheets for fields applied parallel to the c axis.

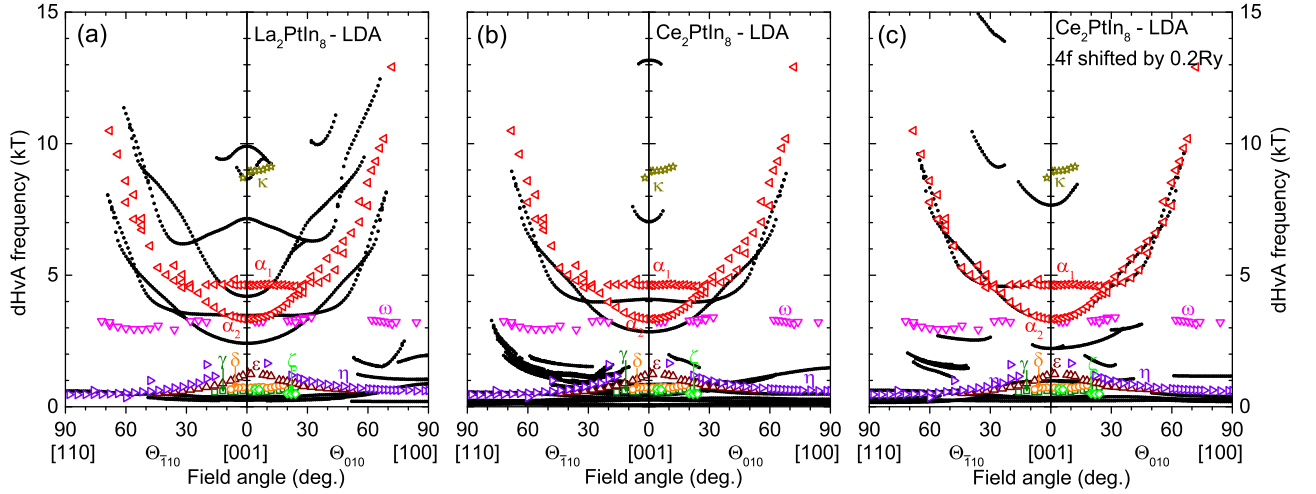


FIG. 7. Comparison of experimental dHvA frequencies of Ce_2PtIn_8 (open symbols) with calculated extremal cross sections (solid circles) of (a) La_2PtIn_8 , (b) Ce_2PtIn_8 , and (c) Ce_2PtIn_8 with shifted $4f$ states. Calculated dHvA frequencies lower than 200 T are not shown for clarity.

the branch ω with the dHvA frequency of about 3 kT. Considering the tetragonal crystal structure with a c/a ratio of about 2.6, near-spherical FS pockets of this size are unexpected. The highest frequency, κ , appears only close to the c axis. It was observed only for the rotation from $[001]$ to $[100]$ direction, because we used a thinner and, therefore, more sensitive cantilever for small angles within this plane.

Due to the layered structure of La_2PtIn_8 and Ce_2PtIn_8 , both the calculations for localized and for itinerant $4f$ electrons suggest the existence of quasi-2D FSs. The main difference, however, is that the calculation for localized $4f$ electrons predicts the existence of two quasi-2D FSs, opposed to only one in the calculation for itinerant $4f$ electrons (see Fig. 6). Since 2D FSs feature a favorable curvature factor and a $1/\cos(\Theta)$ angular dependence of their extremal cross section, they are easily detectable by torque magnetometry. Therefore, the experimental observation of only one 2D FS sheet with extremal areas α_1 and α_2 strongly supports the calculation for itinerant $4f$ electrons. Moreover, the direct comparison of the experimental data with the La_2PtIn_8 calculations, shown in Fig. 7(a), yields a very poor agreement. In particular, none of the observed smaller dHvA frequencies $\gamma \dots \eta$ can be attributed to a calculated branch, especially near the c axis. For α , there is a calculated branch exhibiting a similar angular dependence, but the frequencies differ by about 1 kT.

In contrast, most of the high- and low-frequency experimental branches are reproduced by the Ce_2PtIn_8 calculations, as shown in Fig. 7(b). All the low frequencies $\gamma \dots \eta$ are in good qualitative agreement with calculated ones. More importantly, the frequency associated with the almost cylindrical FS sheet, α , is in very good qualitative agreement with the corresponding calculated branch. We could further improve the quantitative agree-

ment of the quasi-2D FS sheet by shifting the $4f$ states by 0.2 Ry, as depicted in Fig. 7(c). However, there are also a few mismatches. Several calculated branches originating from band 72 were not observed experimentally. Presumably, this is due to an unfavorable curvature factor. We note, that the calculated frequency branches from band 72 were not observed in the isostructural compound Ce_2PdIn_8 as well³⁹.

The frequencies ω and κ are not explained by theory. Assuming an epitaxial growth of the CeIn_3 impurities in our crystal, ω coincides with the frequency branch d of CeIn_3 ¹⁵, rendering CeIn_3 impurities to be the most likely source of ω . On the other hand, the origin of κ is yet unknown. Since the angular dependence of this branch does not reflect the cubic symmetry of CeIn_3 and does not coincide with any of the known frequency branches of CeIn_3 , it appears unlikely for κ to originate from the CeIn_3 impurity. However, the $\text{Ce}_3\text{PtIn}_{11}$ impurity phase, also present in our sample, cannot be ruled out as a possible source of the branch κ . Quantum-oscillation or ARPES measurements of $\text{Ce}_3\text{PtIn}_{11}$ are required to verify this hypothesis. Apart from the aforementioned branches, the band-structure calculations for Ce_2PtIn_8 with shifted $4f$ -electron bands yield an excellent agreement with the experimental data, strongly suggesting itinerant Ce- $4f$ electrons in this compound.

D. Comparison with Pr_2PtIn_8

It would be desirable to directly compare the dHvA oscillations in Ce_2PtIn_8 with those measured in La_2PtIn_8 in order to establish the localized or itinerant character of the Ce- $4f$ electrons beyond any doubts. However, single crystals of La_2PtIn_8 are currently unavailable, rendering a direct comparison impossible. Since the Pr-based ana-

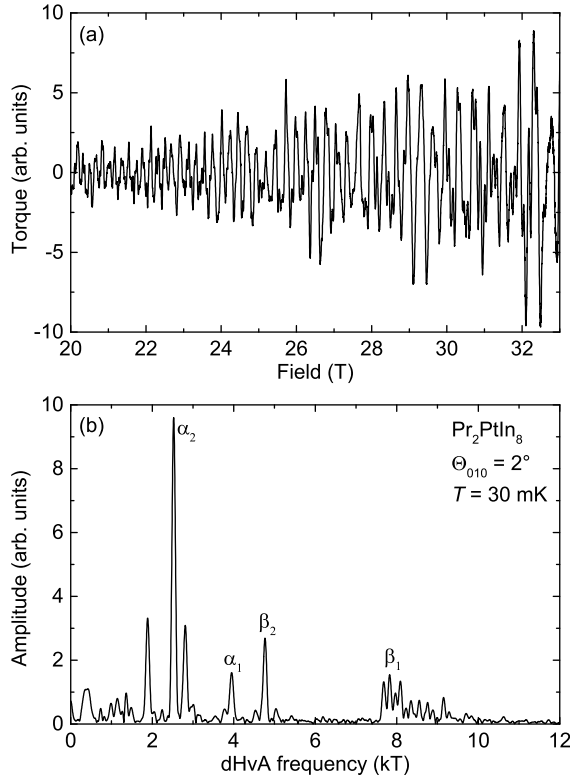


FIG. 8. (a) Torque signal of Pr_2PtIn_8 after subtracting a non-oscillatory background, taken at the same angle as the signal for Ce_2PtIn_8 shown in Fig. 3. (b) Corresponding frequency spectrum obtained by a Fourier transform of the data shown in (a).

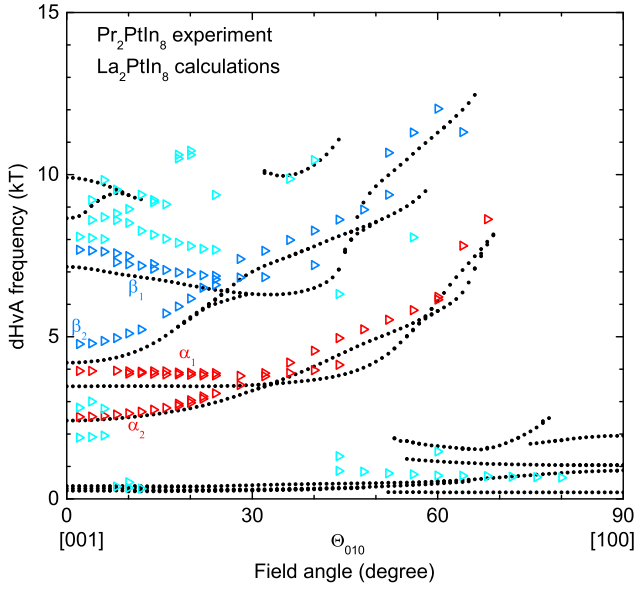


FIG. 9. Comparison of the experimental dHvA frequencies of Pr_2PtIn_8 (open symbols) with calculated extremal cross sections (solid circles) of La_2PtIn_8 .

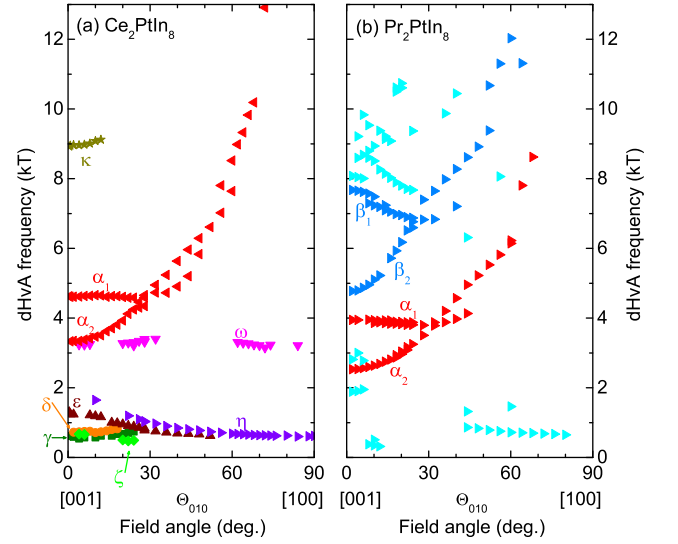


FIG. 10. Angular dependence of the experimental dHvA frequencies in (a) Ce_2PtIn_8 and (b) Pr_2PtIn_8 .

logues of Ce-based HF compounds are known to have localized $4f$ electrons, e.g. in PrCoIn_5 ⁴⁰, Pr_2PtIn_8 poses an alternative candidate for comparison. We, therefore, performed dHvA measurements on Pr_2PtIn_8 . In addition, we conducted specific-heat measurements on our Pr_2PtIn_8 single crystal, revealing a Sommerfeld coefficient of $\gamma = 90 \text{ mJ/molK}^2$. This evidences greatly reduced electronic correlations in Pr_2PtIn_8 compared to Ce_2PtIn_8 , as expected for localized $4f$ electrons.

Figure 8(a) shows a typical torque signal for Pr_2PtIn_8 , after subtracting the non-oscillatory background, taken at the same angle, $\Theta_{010} = 2^\circ$, as shown in Fig. 3 for Ce_2PtIn_8 . The corresponding dHvA frequency spectrum in Fig. 8(b) is clearly different from the one in Fig. 3(b), suggesting different topologies of the FSs of Ce_2PtIn_8 and Pr_2PtIn_8 . In order to verify the consistency, Fig. 9 compares calculated frequencies for $4f$ -localized La_2PtIn_8 with the experimental data of Pr_2PtIn_8 . Indeed, there is a very good agreement between the two data sets. All the large FS sheets calculated for bands 71, 72, and 73 are qualitatively supported by the experimental data. Thus, both the results of the La_2PtIn_8 band-structure calculations and the Pr_2PtIn_8 dHvA measurements are a good reference for $4f$ -localized Ce_2PtIn_8 .

When juxtaposing the angular dependences of Ce_2PtIn_8 and Pr_2PtIn_8 , clear FS differences become even more obvious, as shown in Fig. 10. Apart from parts of the branch η , none of the branches of Ce_2PtIn_8 can be found in Pr_2PtIn_8 . Consequently, the electronic states in Ce_2PtIn_8 differ from those in the $4f$ -localized Pr_2PtIn_8 , further proving the itinerant character of the Ce- $4f$ electrons in Ce_2PtIn_8 . Although Ce_2PtIn_8 is an intermediate compound between CeIn_3 and CePt_2In_7 from a structural point of view, it does not share their localized Ce- $4f$ character.

E. Effective masses of Ce_2PtIn_8

We determined the effective masses of Ce_2PtIn_8 from the temperature dependence of the dHvA oscillation amplitudes. These amplitudes were measured in the field range of 20 to 34 T, for temperatures between 50 and 500 mK, at the same angle as the data shown in Fig. 3. According to the Lifshitz-Kosevich formula, this dependence is proportional to $x/\sinh x$, where $x = \alpha T m^*/B$ and $\alpha = 14.69 \text{ T/K}^{41}$. Here, m^* represents the effective mass given in multiples of the bare electron mass m_e . Figure 11 shows the fit of the temperature dependence of the oscillatory amplitudes by this formula, yielding m^* as fit parameter. The results are summarized in Table I, where the band masses, m_b , obtained from band-structure calculations with shifted $4f$ states by taking the derivative dF/dE , are also shown.

The effective masses are fairly large, ranging from $3.3m_e$ for γ to $25.7m_e$ for κ . The higher the mass of a specific orbit, the stronger the damping of the corresponding oscillation by impurity scattering⁴¹. Given the strongly enhanced effective mass of the κ branch, it seems unlikely that it originates from the $\text{Ce}_3\text{PtIn}_{11}$ impurity, because it would require a very high crystal quality of the impurity itself. Similarly, we observed the impurity frequency ω only for field directions where its effective mass is as small as $2m_e$ ¹⁵.

The measured effective masses exceed the calculated band masses by about an order of magnitude or more. This implies that there is a significant mass enhancement due to many-body interactions, which are not included in the LDA calculations. Effective masses much higher than calculated were observed in other non-magnetic HF compounds with itinerant $4f$ electrons, such as CeCoIn_5 ⁹ and Ce_2PdIn_8 ³⁹. For the α_1 and α_2 orbits, both lying on the same FS sheet, the mass-enhancement factors are 9.5 and 30, respectively. Such largely different mass enhancements on a single FS sheet were also found in CeCoIn_5 ⁹ and CeIrIn_5 ⁴². In CeCoIn_5 , the effective masses were reported to strongly decrease with magnetic field⁹. Similarly, the Sommerfeld coefficient of the specific heat in Ce_2PdIn_8 is strongly suppressed by magnetic field⁴³. This is due to a close proximity to a QCP of these two compounds. In Ce_2PtIn_8 , on the contrary, we have not observed any appreciable field dependence of the effective masses over the field range 16–34 T of our measurements. This suggests that Ce_2PtIn_8 is located further away from a QCP.

In comparison to AFM CeIn_3 ($m^* = 2 \dots 12m_e$ ^{15,44}) and CePt_2In_7 ($m^* = 1.3 \dots 6.2m_e$ ^{17,19}) with localized $4f$ electrons, the effective masses in Ce_2PtIn_8 are significantly higher. Again, this reflects the itinerant character of the Ce- $4f$ electrons, leading to an increased density of states at the Fermi level and stronger many-body interactions.

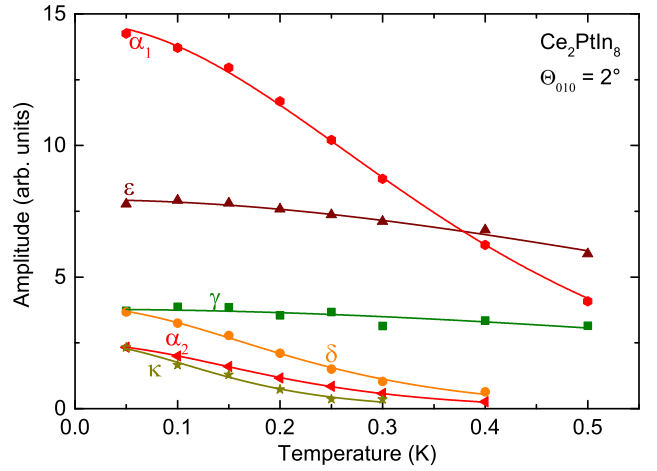


FIG. 11. Temperature-dependent amplitudes, taken at the same angle as the data shown in Fig. 3, with fit lines by use of the Lifshitz-Kosevich formula⁴¹.

Branch	Experiment		Calculation	
	F (kT)	m^* (m_e)	F (kT)	m_b (m_e)
			0.227	0.67
			0.337	0.35
			0.355	0.25
γ	0.55	3.3(1)		
δ	0.73	15.0(3)		
			0.983	1.46
ϵ	1.24	4.6(1)		
			2.222	2.14
α_2	3.34	19.2(1)	3.357	0.61
α_1	4.62	10.5(2)	4.719	1.00
			7.676	1.64
κ	8.99	25.7(10)		

TABLE I. Experimental and calculated (with shifted $4f$ states) dHvA frequencies and effective masses of Ce_2PtIn_8 for $\Theta_{010} = 2^\circ$. Branch assignments refer to Fig. 7.

F. Fermi-surface dimensionality

In order to quantify the degree of deviation from ideal two-dimensionality, we previously introduced the value $\Delta = (S_{max} - S_{min})/S_{avg}$ ³⁹. Here, S_{min} , S_{avg} , and S_{max} are the minimum, average, and maximum cross sections of a quasi-2D FS sheet, respectively. Due to the fact that the observed dHvA frequencies are proportional to the extremal cross sections, we can calculate Δ from our experimental data.

As shown in Fig. 6, one of the calculated FS sheets of Ce_2PtIn_8 is nearly cylindrical. The observation of the experimental branch α proves the existence of this 2D sheet [see Fig. 7(b)]. For this FS sheet, we find a value of $\Delta = 0.32$. This compares to 0.04, 0.03, and 0.07 for the three cylindrical sheets of CePt_2In_7 ¹⁹. Also in the

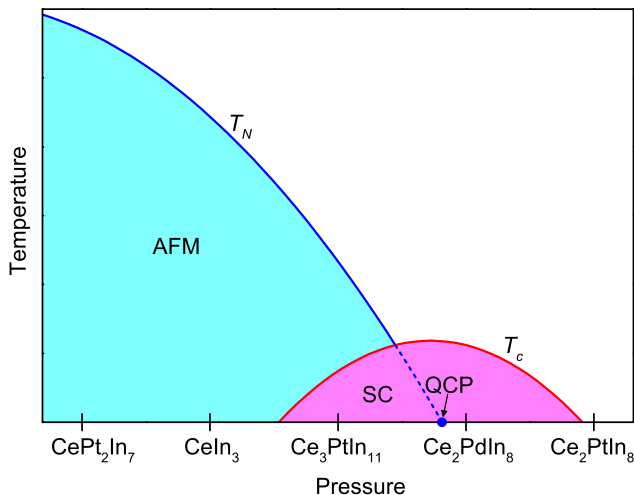


FIG. 12. Schematic location of Ce_2PtIn_8 and other $\text{Ce}_n\text{T}_m\text{In}_{3n+2m}$ compounds in the generic phase diagram of AFM QCPs in Ce-based HF systems. Note that CePt_2In_7 and CeIn_3 were arranged according to their critical pressures (≈ 3.3 and 2.5 GPa, respectively), but not according to their Néel temperatures (5.5 and 10 K, respectively)^{4,20–22}. Ce_2PtIn_8 and Ce_2PdIn_8 were arranged according to their unit cell volumes¹².

prototypical compound, CeCoIn_5 , the value $\Delta = 0.21$ (averaged from Refs. [9], [10], and [45]) is smaller. Consequently, the FS dimensionality of Ce_2PtIn_8 lies between those of CeIn_3 and CeCoIn_5 , as expected from the intermediate two-dimensionality of the crystal structure.

IV. CONCLUSIONS

In summary, we conducted measurements of the dHvA effect on the HF compound Ce_2PtIn_8 and its $4f$ -localized counterpart Pr_2PtIn_8 . By contrasting the data of these two compounds and by comparing the Ce_2PtIn_8 data to band-structure calculations, we find clear evidence for itinerant Ce- $4f$ electrons in this material. In addition, the effective masses are strongly enhanced, varying between $3.3m_e$ and $25.7m_e$ for the different FS sheets.

Structurally, Ce_2PtIn_8 can be considered as an intermediate compound between CeIn_3 and CePt_2In_7 . The FSs of Ce_2PtIn_8 follow the structural trend, being less 2D than those of CePt_2In_7 , but more than those of CeIn_3 . Both CeIn_3 and CePt_2In_7 have localized Ce- $4f$ electrons, in contrast to Ce_2PtIn_8 . It is, therefore, not surprising that the effective masses in Ce_2PtIn_8 are considerably enhanced.

There are a lot of similarities between the electronic structures of Ce_2PtIn_8 and the isostructural Ce_2PdIn_8 ³⁹. All the FS sheets of Ce_2PtIn_8 correspond to almost identical sheets in Ce_2PdIn_8 . The only exception are very small FS pockets originating from band 74 of Ce_2PdIn_8 ³⁹, which cannot be found in Ce_2PtIn_8 . Both compounds

feature enhanced effective masses and itinerant $4f$ electrons.

In the generic temperature-pressure phase diagram of Ce-based HF compounds, the AFM ordering temperature T_N decreases upon increasing pressure⁴⁶, as shown in Fig. 12. At $T = 0$ and the critical pressure P_c , a QCP separates the AFM and the paramagnetic phases. The f electrons of Ce are usually found to be localized in the former, and itinerant in the latter^{14,47,48}. The superconducting dome is located around this critical pressure. In Ce_2PdIn_8 , for example, the observation of a non-Fermi-liquid behavior at low temperature^{43,49–54} suggests the close proximity to a QCP.

Our data reveal the $4f$ -itinerant ground state of Ce_2PtIn_8 , and no signatures of a superconducting transition. This is not surprising, given that Ce_2PtIn_8 has a smaller unit cell volume than Ce_2PdIn_8 ¹², but very similar FSs. Consequently, Ce_2PtIn_8 can be considered a compressed version of Ce_2PdIn_8 . Altogether, this suggests that in the temperature-pressure phase diagram, Ce_2PtIn_8 is located outside the superconducting dome at pressures larger than P_c (see Fig. 12). Thus, we assume that a negative pressure induced by chemical substitution would tune Ce_2PtIn_8 to an AFM QCP, similar to $\text{CeCu}_{6-x}\text{Au}_x$ ^{55–57} or $\text{Ce}_{1-x}\text{La}_x\text{Ru}_2\text{Si}_2$ ⁵⁸.

In Ref. [39], we found a trend between the FS dimensionality and the superconducting T_c of several Ce-based HF compounds. The corrugated cylindrical FS sheet of Ce_2PtIn_8 ($\Delta = 0.32$) deviates less from ideal two-dimensionality than the corresponding sheet in Ce_2PdIn_8 ($\Delta = 0.39$)³⁹. Therefore, one could expect to observe superconductivity in Ce_2PtIn_8 with a higher T_c than in Ce_2PdIn_8 . However, we have not observed any sign of superconductivity in Ce_2PtIn_8 in our torque measurements. Since Ce_2PtIn_8 is likely to be located further away from a QCP, we conclude that the proximity to a QCP is essential for superconductivity. The other known members of the $\text{Ce}_n\text{Pt}_m\text{In}_{3n+2m}$ family can be tuned to a QCP by applying pressure. With increasing structural two-dimensionality, their respective T_c 's at the QCP increase from 0.2 K (CeIn_3 ⁴) to 0.7 K ($\text{Ce}_3\text{PtIn}_{11}$ ²³) to 2.1 K (CePt_2In_7 ^{20–22}). For CeIn_3 ^{14–16}, Ce_2PtIn_8 (this work), and CePt_2In_7 ^{17–19}, the FS dimensionality follows the structural dimensionality. Assuming that the FSs of $\text{Ce}_3\text{PtIn}_{11}$ also follow this trend, this indicates that quasi-2D FSs may enhance the T_c observed at the QCP. An investigation of the $\text{Ce}_3\text{PtIn}_{11}$ FSs would be desirable to verify this trend.

V. ACKNOWLEDGMENTS

We acknowledge the support of the LNCMI-CNRS, and the HLD-HZDR, members of the European Magnetic Field Laboratory (EMFL), ANR-DFG grant “FermiNEst”, JSPS KAKENHI Grants No. JP15H05882, No. JP15H05884, No. JP15H05886, No. JP15K21732 (J-Physics), and JP16H02450. K.G. acknowledges support from the DFG within GRK 1621.

- * j.klotz@hzdr.de
- † Present address: Department of Physics, University of Warwick, Coventry, CV4 7AL, United Kingdom
ilya.sheikin@lncmi.cnrs.fr
- ¹ C. Petrovic, P. G. Pagliuso, M. F. Hundley, R. Movshovich, J. L. Sarrao, J. D. Thompson, Z. Fisk, and P. Monthoux, *J. Phys.: Condens. Matter* **13**, L337 (2001).
 - ² S. Ikeda, H. Shishido, M. Nakashima, R. Settai, D. Aoki, Y. Haga, H. Harima, Y. Aoki, T. Namiki, H. Sato, and Y. Ōnuki, *J. Phys. Soc. Jpn.* **70**, 2248 (2001).
 - ³ T. Moriya, Y. Takahashi, and K. Ueda, *J. Phys. Soc. Jpn.* **59**, 2905 (1990).
 - ⁴ N. D. Mathur, F. M. Grosche, S. R. Julian, I. R. Walker, D. M. Freye, R. K. W. Haselwimmer, and G. G. Lonzarich, *Nature* **394**, 39 (1998).
 - ⁵ P. Monthoux and G. G. Lonzarich, *Phys. Rev. B* **59**, 14598 (1999).
 - ⁶ P. Monthoux, *J. Phys.: Condens. Matter* **15**, S1973 (2003).
 - ⁷ P. Monthoux, D. Pines, and G. G. Lonzarich, *Nature* **450**, 1177 (2007).
 - ⁸ H. Shishido, T. Shibauchi, K. Yasu, T. Kato, H. Kontani, T. Terashima, and Y. Matsuda, *Science* **327**, 980 (2010).
 - ⁹ R. Settai, H. Shishido, S. Ikeda, Y. Murakawa, M. Nakashima, D. Aoki, Y. Haga, H. Harima, and Y. Onuki, *J. Phys.: Condens. Matter* **13**, L627 (2001).
 - ¹⁰ D. Hall, E. C. Palm, T. P. Murphy, S. W. Tozer, Z. Fisk, U. Alver, R. G. Goodrich, J. L. Sarrao, P. G. Pagliuso, and T. Ebihara, *Phys. Rev. B* **64**, 212508 (2001).
 - ¹¹ T. Nomoto and H. Ikeda, *Phys. Rev. B* **90**, 125147 (2014).
 - ¹² M. Kratochvilova, M. Dusek, K. Uhlířová, A. Rudajevova, J. Prokleška, B. Vondrackova, J. Custers, and V. Sechovsky, *J. Crys. Growth* **397**, 47 (2014).
 - ¹³ Z. M. Kurenbaeva, E. V. Murashova, Y. D. Seropegin, H. Noël, and A. I. Tursina, *Intermetallics* **16**, 979 (2008).
 - ¹⁴ R. Settai, T. Kubo, T. Shiromoto, D. Honda, H. Shishido, K. Sugiyama, Y. Haga, T. D. Matsuda, K. Bet-suyaku, H. Harima, T. C. Kobayashi, and Y. Ōnuki, *J. Phys. Soc. Jpn.* **74**, 3016 (2005).
 - ¹⁵ T. Ebihara, I. Umehara, A. K. Albessard, K. Satoh, and Y. Ōnuki, *Physica B* **186**, 123 (1993).
 - ¹⁶ M. Endo, N. Kimura, and H. Aoki, *J. Phys. Soc. Jpn.* **74**, 3295 (2005).
 - ¹⁷ M. M. Altarawneh, N. Harrison, R. D. McDonald, F. F. Balakirev, C. H. Mielke, P. H. Tobash, J.-X. Zhu, J. D. Thompson, F. Ronning, and E. D. Bauer, *Phys. Rev. B* **83**, 081103 (2011).
 - ¹⁸ A. Miyake, Y. Kohama, S. Ohta, Y. Hirose, R. Settai, K. Matsubayashi, Y. Uwatoko, A. Matsuo, K. Kindo, and M. Tokunaga, *J. Phys.: Conf. Ser.* **592**, 012149 (2015).
 - ¹⁹ K. Götze, Y. Krupko, J. A. N. Bruin, J. Klotz, R. D. H. Hinlopen, S. Ota, Y. Hirose, H. Harima, R. Settai, A. McCollam, and I. Sheikin, *Phys. Rev. B* **96**, 075138 (2017).
 - ²⁰ E. D. Bauer, H. O. Lee, V. A. Sidorov, N. Kurita, K. Gofryk, J.-X. Zhu, F. Ronning, R. Movshovich, J. D. Thompson, and T. Park, *Phys. Rev. B* **81**, 180507 (2010).
 - ²¹ V. A. Sidorov, X. Lu, T. Park, H. Lee, P. H. Tobash, R. E. Baumbach, F. Ronning, E. D. Bauer, and J. D. Thompson, *Phys. Rev. B* **88**, 020503 (2013).
 - ²² S. Kurahashi, S. Ota, S. Tomaru, Y. Hirose, and R. Settai, *J. Phys.: Conf. Ser.* **592**, 012006 (2015).
 - ²³ J. Prokleška, M. Kratochvilová, K. Uhlířová, V. Sechovský, and J. Custers, *Phys. Rev. B* **92**, 161114 (2015).
 - ²⁴ D. Kaczorowski, A. P. Pikul, D. Gnida, and V. H. Tran, *Phys. Rev. Lett.* **103**, 027003 (2009).
 - ²⁵ K. Uhlířová, J. Prokleška, and V. Sechovský, *Phys. Rev. Lett.* **104**, 059701 (2010).
 - ²⁶ D. Kaczorowski, A. P. Pikul, D. Gnida, and V. H. Tran, *Phys. Rev. Lett.* **104**, 059702 (2010).
 - ²⁷ K. Uhlířová, J. Prokleška, V. Sechovský, and S. Daniš, *Intermetallics* **18**, 2025 (2010).
 - ²⁸ D. Kaczorowski, D. Gnida, A. P. Pikul, and V. H. Tran, *Solid State Commun.* **150**, 411 (2010).
 - ²⁹ G. Chen, S. Ohara, M. Hedo, Y. Uwatoko, K. Saito, M. Sorai, and I. Sakamoto, *J. Phys. Soc. Jpn.* **71**, 2836 (2002).
 - ³⁰ M. Nicklas, V. A. Sidorov, H. A. Borges, P. G. Pagliuso, C. Petrovic, Z. Fisk, J. L. Sarrao, and J. D. Thompson, *Phys. Rev. B* **67**, 020506 (2003).
 - ³¹ T. Ueda, H. Shishido, S. Hashimoto, T. Okubo, M. Yamada, Y. Inada, R. Settai, H. Harima, A. Galatanu, E. Yamamoto, N. Nakamura, K. Sugiyama, T. Takeuchi, K. Kindo, T. Namiki, Y. Aoki, H. Sato, and Y. Ōnuki, *J. Phys. Soc. Jpn.* **73**, 649 (2004).
 - ³² J. D. Thompson, R. Movshovich, Z. Fisk, F. Bouquet, N. J. Curro, R. A. Fisher, P. C. Hammel, H. Hegger, M. F. Hundley, M. Jaime, P. G. Pagliuso, C. Petrovic, N. E. Phillips, and J. L. Sarrao, *J. Magn. Magn. Mater.* **226**, 5 (2001).
 - ³³ J. S. Kim, N. O. Moreno, J. L. Sarrao, J. D. Thompson, and G. R. Stewart, *Phys. Rev. B* **69**, 024402 (2004).
 - ³⁴ S. Raj, Y. Iida, S. Souma, T. Sato, T. Takahashi, H. Ding, S. Ohara, T. Hayakawa, G. F. Chen, I. Sakamoto, and H. Harima, *Phys. Rev. B* **71**, 224516 (2005).
 - ³⁵ S. Souma, S. Raj, J. C. Campuzano, T. Sato, T. Takahashi, S. Ohara, and S. Sakamoto, *Physica B* **403**, 752 (2008).
 - ³⁶ R. Jiang, D. Mou, C. Liu, X. Zhao, Y. Yao, H. Ryu, C. Petrovic, K.-M. Ho, and A. Kaminski, *Phys. Rev. B* **91**, 165101 (2015).
 - ³⁷ H. Shishido, T. Yoshihara, D. Nagamiya, S. Noguchi, H. Fujiwara, and T. Ishida, *J. Phys.: Conf. Ser.* **592**, 012007 (2015).
 - ³⁸ D. D. Koelling and B. N. Harmon, *J. Phys. C: Solid State Phys.* **10**, 3107 (1977).
 - ³⁹ K. Götze, J. Klotz, D. Gnida, H. Harima, D. Aoki, A. Demuer, S. Elgazzar, J. Wosnitza, D. Kaczorowski, and I. Sheikin, *Phys. Rev. B* **92**, 115141 (2015).
 - ⁴⁰ S. Elgazzar, I. Opahle, M. Richter, and P. M. Oppeneer, *Phys. Rev. B* **77**, 125105 (2008).
 - ⁴¹ D. Shoenberg, *Magnetic Oscillations in Metals* (Cambridge University Press, Cambridge, UK, 1984).
 - ⁴² Y. Haga, Y. Inada, H. Harima, K. Oikawa, M. Murakawa, H. Nakawaki, Y. Tokiwa, D. Aoki, H. Shishido, S. Ikeda, N. Watanabe, and Y. Ōnuki, *Phys. Rev. B* **63**, 060503 (2001).
 - ⁴³ Y. Tokiwa, P. Gegenwart, D. Gnida, and D. Kaczorowski, *Phys. Rev. B* **84**, 140507 (2011).
 - ⁴⁴ I. Umehara, Y. Kurosawa, M. Kikuchi, N. Nagai, K. Satoh, and Y. Onuki, *Physica B* **165**, 331 (1990).
 - ⁴⁵ A. Polyakov, O. Ignatchik, B. Bergk, K. Götze, A. D. Bianchi, S. Blackburn, B. Prévost, G. Seyfarth, M. Côté, D. Hurt, C. Capan, Z. Fisk, R. G. Goodrich, I. Sheikin, M. Richter, and J. Wosnitza,

- Phys. Rev. B **85**, 245119 (2012).
- ⁴⁶ J. Flouquet, D. Aoki, F. Bourdarot, F. Hardy, E. Hassinger, G. Knebel, T. D. Matsuda, C. Meingast, C. Paulsen, and V. Taufour, J. Phys.: Conf. Ser. **273**, 012001 (2011).
 - ⁴⁷ S. Araki, R. Settai, T. C. Kobayashi, H. Harima, and Y. Ōnuki, Phys. Rev. B **64**, 224417 (2001).
 - ⁴⁸ H. Shishido, R. Settai, H. Harima, and Y. Ōnuki, J. Phys. Soc. Jpn. **74**, 1103 (2005).
 - ⁴⁹ J. K. Dong, H. Zhang, X. Qiu, B. Y. Pan, Y. F. Dai, T. Y. Guan, S. Y. Zhou, D. Gnida, D. Kaczorowski, and S. Y. Li, Phys. Rev. X **1**, 011010 (2011).
 - ⁵⁰ V. H. Tran, D. Kaczorowski, R. T. Khan, and E. Bauer, Phys. Rev. B **83**, 064504 (2011).
 - ⁵¹ D. Gnida, M. Matusiak, and D. Kaczorowski, Phys. Rev. B **85**, 060508 (2012).
 - ⁵² M. Matusiak, D. Gnida, and D. Kaczorowski, Phys. Rev. B **84**, 115110 (2011).
 - ⁵³ H. Fukazawa, R. Nagashima, S. Shimatani, Y. Kohori, and D. Kaczorowski, Phys. Rev. B **86**, 094508 (2012).
 - ⁵⁴ V. H. Tran, A. D. Hillier, D. T. Adroja, and D. Kaczorowski, Phys. Rev. B **86**, 094525 (2012).
 - ⁵⁵ A. Germann, A. K. Nigam, J. Dutzi, A. Schröder, and H. v. Löhneysen, J. Phys. Colloques **49**, C8 (1988).
 - ⁵⁶ M. R. Lees and B. R. Coles, J. Magn. Magn. Mater. **76**, 173 (1988).
 - ⁵⁷ A. Germann and H. v. Löhneysen, Europhys. Lett. **9**, 367 (1989).
 - ⁵⁸ M. J. Besnus, P. Lehmann, and A. Meyer, J. Magn. Magn. Mater. **63**, 323 (1987).